A&A 388, 1048–1061 (2002)
DOI: 10.1051/0004-6361:20020542

Astronomy & Astrophysics

Sunspot photometry with phase diversity

II. Fine-structure characteristics

A. Tritschler and W. Schmidt

Kiepenheuer–Institut für Sonnenphysik, Schöneckstr. 6, 79104 Freiburg, Germany
e-mail: ali, wolfgang@kis.uni-freiburg.de

Received 12 November 2001 / Accepted 8 April 2002

Abstract. We investigate the thermal and morphological fine structure of a small sunspot, which includes the determination of brightness temperatures and characteristic spatial scales as well as their distribution inside the sunspot. The identification and isolation of sunspot fine structure is accomplished by means of a feature-finding algorithm applied to a high-resolution time sequence taken simultaneously in three continuum bands of the solar spectrum. In order to compensate for seeing and instrumental effects, we apply the phase-diversity technique combined with a deconvolution method. The findings can be summarized as follows: (1) umbral dots are found to be on average 760 K cooler than the immediate surrounding photosphere outside the spot. (2) Some exceptional hot penumbral grains exceed the average temperature of the brightest granules of the spots surroundings by typically 150 K. (3) The size distribution of umbral dots and penumbral grains support the idea that the smallest structures are still spatially unresolved. (4) The distribution function of umbral dot peak intensities points to the existence of two umbral dot "populations" indicating different efficiency of energy transport. (5) The classification of penumbral filaments into "dark" and "bright" depends on the immediate surroundings.

Key words. Sun: sunspots – techniques: image processing

1. Introduction

Umbral dots (UDs) are point-like bright features inside the umbra. They are irregularly distributed inside the umbral regions, but this distribution is far from random. UDs cover from 6–18% of the umbral area in dependence on identification criteria, data quality and data type (spectra or filtergram) and sunspot brightness (Adjabshirzadeh & Koutchmy 1983; Pahlke & Wiehr 1990; Sobotka et al. 1993, 1997a). The appearance and brightness of UDs is closely related to the properties of the local umbral background (Sobotka et al. 1992a,b, 1993). Measured UD-brightnesses vary on a broad range between 0.08 $I^{\odot}$–0.90 $I^{\odot}$ (Sobotka et al. 1993, 1997b) and UD-temperatures are found typically to lie below the temperature of the mean quiet sun (Grossmann-Doerth et al. 1986; Bumba et al. 1990; Pahlke & Wiehr 1990; Aballe-Villero 1991; Sütterlin & Wiehr 1998). However, exceptional high UD temperatures, close to the mean quiet sun, derived from a two-colour photometry are reported by Beckers & Schröter (1968) and Koutchmy & Adjabshirzadeh (1981). Observed UD sizes vary between 0.2–1.4 arcsec (Beckers & Schröter 1968; Adjabshirzadeh & Koutchmy 1978, 1980, 1983; Koutchmy & Adjabshirzadeh 1981; Grossmann-Doerth et al. 1986; Aballe-Villero 1991; Sobotka et al. 1993, 1997a). There is evidence that UDs are not spatially resolved, so that the size distribution function increases towards the diffraction limit given by the telescope (Sobotka et al. 1997a). Thus, the smaller the UDs, the more numerous they are, or, in other words, no characteristic size of UDs can be given, because the size seems to concentrate below the diffraction limit of the respective measurement.

Although UDs are conspicious in brightness and temperature, they are rather unspectacular in other physical parameters. Observationally, magnetic fields in UDs are not substantially weaker than those of the umbral surroundings. Measured magnetic field reductions on spatial scales corresponding to the observed UDs are in the range 1–20% (Adjabshirzadeh & Koutchmy 1983; Pahlke & Wiehr 1990; Lites et al. 1991; Wiehr & Degenhardt 1993; Schmidt & Balthasar 1994; Tritschler & Schmidt 1997). There is no evidence of a significant velocity difference between UDs and the surrounding umbral regions (Pahlke & Wiehr 1990; Lites et al. 1991; Wiehr 1994; Schmidt & Balthasar 1994). Thus, UDs are magnetically and dynamically (vertical flows) "invisible" and nearly undistinguishable from the properties of the umbral surroundings. This is in contradiction to common ideas of

Send offprint requests to: A. Tritschler,
e-mail: ali@kis.uni-freiburg.de

sunspot umbral structure, which cover mainly the cluster model or follow magnetoconvective beliefs.

Within the framework of the cluster model UDs are identified with intrusions of field free hotter fluid channeled between the flux tubes that are darkened due to the suppression of convection by the magnetic field (Obridko 1975; Parker 1979a,b; Choudhuri 1986). Before reaching the photosphere the magnetic field lines are closed at the top of the intrusions. The hot plasma inside the field free regions piles up and leads to a local increase of temperature and pressure. Thus the column rises vertically as a whole until the photosphere is reached where the pressure drops drastically and the magnetic field lines are no longer able to close at the top of the column. The plasma leaks out through a "magnetic valve". The UD decays when the pressure inside decreases sufficiently so that the surrounding magnetic field closes again.

In the context of a magnetoconvective model UDs are interpreted as the top of convective cells present in a homogeneous vertical magnetic field (Knobloch & Weiss 1984). The presence of a strong magnetic field modifies the nature of convection substantially. What convection looks like depends critically on the parameter ζ, the ratio of magnetic to thermal diffusivity. For $\zeta < 1$ oscillatory convection occurs in the upper sunspot layers, while steady convection evolves only in the deeper sunspot layers. Numerical simulations of two-dimensional magnetoconvection show that oscillatory and steady convection couple in such a way that one gets hot regions of upwelling gas with somewhat dispersed magnetic field (Weiss et al. 1990).

However, the obvious resemblance between the two models is, that UDs in either picture tend to weaken the magnetic fields and are connected with an upward motion. Both properties are not observed. How to reconcile observations with the predictions of the models? Lites et al. (1991) first pointed out that the contradiction with existing observations may be due to some point to the fact that in both models radiative transfer is neglected. Radiative transfer is important in the upper layers of a sunspot, where the opacity becomes small. Upward motions are probably damped out in these layers due to considerable amount of energy being lost by radiative transfer. The lack of upward flow excludes the UD to be interpreted as Choudhuris magnetic valve, but the UD can still be the upper part of the tapering column, from which the energy leaks out due to efficient radiative transfer. Thus, the reduction of the magnetic field inside the UD is not observable, because the measurements are not done in a line formed below the vertex. The brightness of an UD is due to energy diffusing radiatively from the vertex, resulting in UD temperatures lower than that of the photosphere outside the spot.

In contrast to the still puzzling nature of UDs the penumbra and its fine structure has lost some of its mysteriousness. The recent progress in two-dimensional spectroscopy and spectropolarimetry together with time sequences of high spatial resolution and promising numerical simulations seem to give a concise picture of the penumbral phenomena and its fine structure, which is dominated by the bright penumbral filaments with their comet-like shaped heads – the penumbral grains (PGs) (Muller 1973). Observations of PGs give an average width of 0.35 arcsec and length scales in the range 0.5–2.0 arcsec (Krat et al. 1972; Bruzek 1977; Muller 1973; Moore 1981; Bonet et al. 1982). Grossmann-Doerth & Schmidt (1981) state an upper limit of 0.55 arcsec for bright and dark filaments, whereas analysis of penumbral power spectra indicate significant signal close to the diffraction limit (Harvey & Breckinridge 1973; Stachnik et al. 1983; Lites et al. 1990; Denker et al. 1995). Sanchez Almeida & Bonet (1998a,b) estimate that the real size of penumbral filaments is below the achievable resolution varying on scales of a few kilometers. The brightness of PGs reaches that of the mean surrounding photosphere outside the spot. Individual PGs can even exceed the brightness of the brightest granules (Sütterlin & Wiehr 1998).

The morphological appearance of the penumbra suggests the existence of two components: a bright and a dark component covering ∼43–49% and ∼51–57% of the penumbral region (Muller 1973; Collados et al. 1988). The average brightness of the bright and the dark component is in the range 0.78 $I^{\odot}$–1.07 $I^{\odot}$ and 0.61 $I^{\odot}$–0.79 $I^{\odot}$, respectively (Krat et al. 1972; Grossmann-Doerth & Schmidt 1981; Collados et al. 1988). Contrary to the visual glimpse, the corresponding penumbral intensity distribution reveals a single-peaked shape (Grossmann-Doerth & Schmidt 1981; Collados et al. 1988; Denker 1998). Thereafter the term bright and dark filament is of only local meaning and penumbral filaments are defined by their immediate surroundings. However, Collados et al. (1988) show with a simple two-component model that this is not in direct contradiction to the existence of two components.

In accordance with magneto-hydrodynamical simulations, the penumbral structure is stamped by the dynamcis of ascending flux tubes (Schlichenmaier et al. 1998). In this picture, the PGs are interpreted as the foot points of flux tubes. The flux tubes, heated by a systematic flow (Evershed flow), establish temperatures even higher than the hottest granules in the surrounding photosphere outside the spot. The optically thick bright filaments correspond to the radiative signature of the horizontally outflowing hot plasma channeled by the flux tube. During the outflow the plasma cools and the original bright filament thins, until it becomes optical thin and cannot be distinguished from the dark background (Schlichenmaier et al. 1999). This gives a natural explanation of the characteristic tail of the bright filaments.

In this investigation we analyze the morphologic properties and brightness of a small sunspot as described in Tritschler & Schmidt (2002) (hereafter: TS). Section 3 introduces the algorithm used to identify and isolate the sunspots small-scale structures. Section 4 presents the results, like umbral and penumbral brightness and size distributions, filling factors, brightness-background relations

and brightness-size relations. In Sect. 5 the results are discussed and compared to already existing observations. A summary of our findings is given in Sect. 5.

2. Observations and data reduction

Observations were made on May 19, 1995, with the German Vacuum Tower Telescope (VTT) located at the Observatorio del Teide on Tenerife. In order to observe simultaneously in three different continuum bands (402.1 nm, 569.5 nm and 709.1 nm) of the solar spectrum, the observations also employed the Multichannel Filter System of the VTT (Kentischer 1995). To apply the phase-diversity technique, a defocused image was taken additionally in one of the wavelength channels (569.5 nm, phase-diversity channel).

The analyzed data set covers a ∼90 min sequence of a well developed sunspot (NOAA 7871, f-spot, 25 arcsec in diameter), observed out of disc center ($\mu = 0.79$).

First steps of the analysis included gain correction and subtraction of dark current. For more details of the observation, the calibration process and the image reconstruction and processing methods see TS.

3. Identification of sunspot fine structure

The study of sunspot fine structure covers the consideration of size, brightness and area fraction as well as the distribution of these quantities. This implies the identification and isolation of the relevant features in the umbra and penumbra, which is accomplished by means of a feature-finding algorithm (FFA) working in the following way.

In a first step, for each frame a binary mask is worked out, which defines the umbra and the penumbra (see TS). In a second step, from each frame a smoothed version (boxcar average with size 0.57×0.57 arcsec^2) is subtracted to create a difference image with contrast enhanced fine structure. On the basis of this difference image a binary mask is generated by setting all pixels above a certain intensity threshold (ΔI) equal to 1 and all other pixels equal to 0. This mask is applied to the actual frame. A single structure is thus defined by a contour line – depending on ΔI – in the difference frame. For each identified structure the following parameters are determined: peak intensity, P, average intensity, A, local background intensity, B, and size. The local background intensity, B, results from an intensity average over the adjacent intensity minima next to the structure under consideration. These minimum-contour intensities are denoted with D. The structure size is measured by means of the spatial extent at half of the intensity difference $P-B$ (*FWHM*-area) and is specified in form of an effective diameter $d_{\rm eff}$: the diameter of a circle with the same area. The diffraction limit in the three continua is about 0.144, 0.205 and 0.244 arcsec, respectively, corresponding to a size of ∼2 pixel for the given image scale of 0.0823 arcsec pixel^{-1}. Therefore all structures with a *FWHM*-area < 4, 7, 10 pixel, respectively, are excluded.

Identified structures inside the umbra or penumbra are labeled as UDs or PGs, respectively. At this point we want to make some further comments on the algorithm:

- The identification of structures is very sensitive to the choice of the threshold intensity ΔI. Too small a value implicates that the FFA selects noise. This is prevented by a large ΔI, but at then all low-contrast structures are discarded. Therefore we chose a variable value for ΔI. For the umbra values $\Delta I = 0.01$, 0.015, 0.020, 0.025 and for the penumbra values $\Delta I = 0.020$, 0.025, 0.03 were used. For higher values, the number of structures dropped drastically. The lowest value of ΔI is about 20% above the estimated noise level.
- The identified structures are not traced in time. This constraint is due to the composition of the data set. The relative large time lag between subsequent images of the sequence and the variable seeing conditions aggravate the identification of one and the same feature in different frames, especially inside the umbra. Therefore we did not design the algorithm as a feature-tracking algorithm. In this sense the FFA has no memory, the images are considered as independend from each other. This implies that the set of all identified features also reflects the temporal evolution of the individual constituents.
- The FFA is not a morphological filter. The intensity and not the shape is decisive for the identification of a structure.

If not mentionend otherwise, all statements in the text and the figures in the following sections refer to: (a) structures with a minimum size of 4, 7, 10 pixel; (b) a threshold intensity of $\Delta I = 0.01$ for the umbra and $\Delta I = 0.02$ for the penumbra; (c) the reconstructed data set; (d) the green continuum band (phase-diversity channel). Brightness is given in units of the mean quiet sun, $I^{\odot}$, outside the spot. Since we derive brightness temperatures, the terms intensity, I, and temperature, T, can be regarded as synonyms, although they are different physical quanteties.

4. Fine-structure characteristics

4.1. Brightness temperature

Figure 1 visualizes the relation between the peak intensity P and the mean local background intensity B of the identified features inside the umbra (upper row) and the penumbra (lower row) in the three observed continuum bands. The umbra reveals a sector-shape distribution in the P–B plane. The UD peak intensities and the background intensities are correlated and the correlation decreases with increasing wavelength. The lower edge of the sector depends on the choice of the threshold intensity ΔI:

- High value of ΔI:
  Favoured are the brightest structures that can be clearly distinguished from the background. For a very low background intensity, isolated and very bright

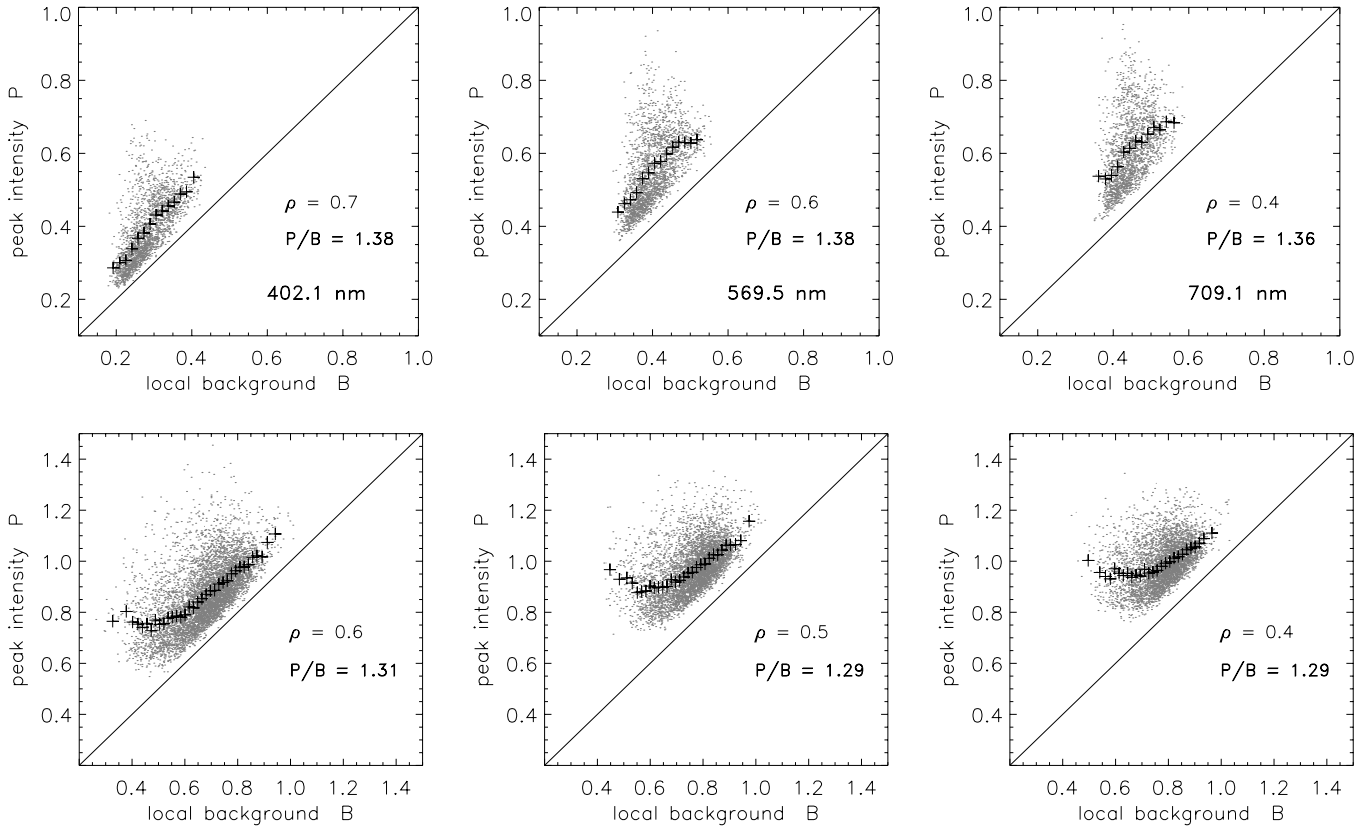

Fig. 1. P–B relation of identified structures in the three observed continuum bands at 402.1 nm, 569.5 nm and 709.1 nm. Upper panel: umbral structures (UDs). Lower panel: penumbral structures (PGs). ρ: linear correlation coefficient between P und B. P/B: over all structures averaged intensity ratio. +: mean peak intensity for a binned background intensity (UDs: bin size = 0.016. PGs: bin size = 0.018).

UDs, located deeply inside the umbra are selected. For a very high background intensity, those UDs are selected which are located in an environment that exhibits a strong intensity gradient.

– Low value of ΔI:
Selected are those UDs, which are hard to distinguish from the background. This affects isolated and weak UDs deep inside the umbra (with a low background intensity) and those UDs, that are located at the boundary to the penumbra (or the lightbridge) or in the neighbourhood of a very bright UD.

None of the identified UDs reaches the brightness of the surrounding photosphere outside the spot: the UD peak intensity P varies in the range 0.36–0.94 (4860–5950 K). The observed UDs are on average ∼37% (330 K) brighter than the mean local background $\overline{B}$ and ∼45% (760 K) darker than the undisturbed photosphere (6040 K). UD-background intensities B vary on the range 0.29–0.55 (4640–5290 K) with an average of $\overline{B} = 0.40 \pm 0.05$ (4950 ± 110 K). With increase of the threshold intensity ΔI the average $\overline{P}$ increases slightly, since low contrast UDs no longer contribute. On average the ratio $\overline{P/B}$ amounts to 1.38 ± 0.21, peak values are almost twice as high ($(P/B)_{\max} = 2.46$).

The penumbra does not show the sector-like distribution in the P–B plane. The individual peak intensities, P, of the PGs and the corresponding background intensities, B, are less correlated than for structures in the umbra. PGs are on average only 3% (50 K) darker than the mean quiet sun. The peak brightness P of individual PGs is in the range 0.71–1.35 (5590–6490 K). The local background brightness is on average 0.76 ± 0.10 (5660 ± 170 K) with individual values between 0.42–1.03 (5000–6080 K). The average ratio $\overline{P/B}$ amounts to 1.3 ± 0.17, whereas exceptional bright PGs reveal a P/B ratio up to 2.77. A summary of all relevant values is given in Table 2 at the end of Sect. 6.

Alternatively, we can take another point of view. For each specified background intensity, B, a range of structure brightness (UD or PG) is observed. Thus, there exist bright as well as faint structures at the same background intensity. Therefore, each background intensity can be assigned a mean intensity, that results from an average over the corresponding range of observed UD or PG brightness. These mean intensities are marked in Fig. 1 with the +-symbol. For reasons of representation binned +-values are plotted.

In Fig. 2 the distribution of the peak intensities, P, the averaged intensities, A, the local background intensities, B, and the individual minimum-contour intensities, D, are displayed for the umbra (upper row) and the penumbra (lower row). The distribution functions refer to the

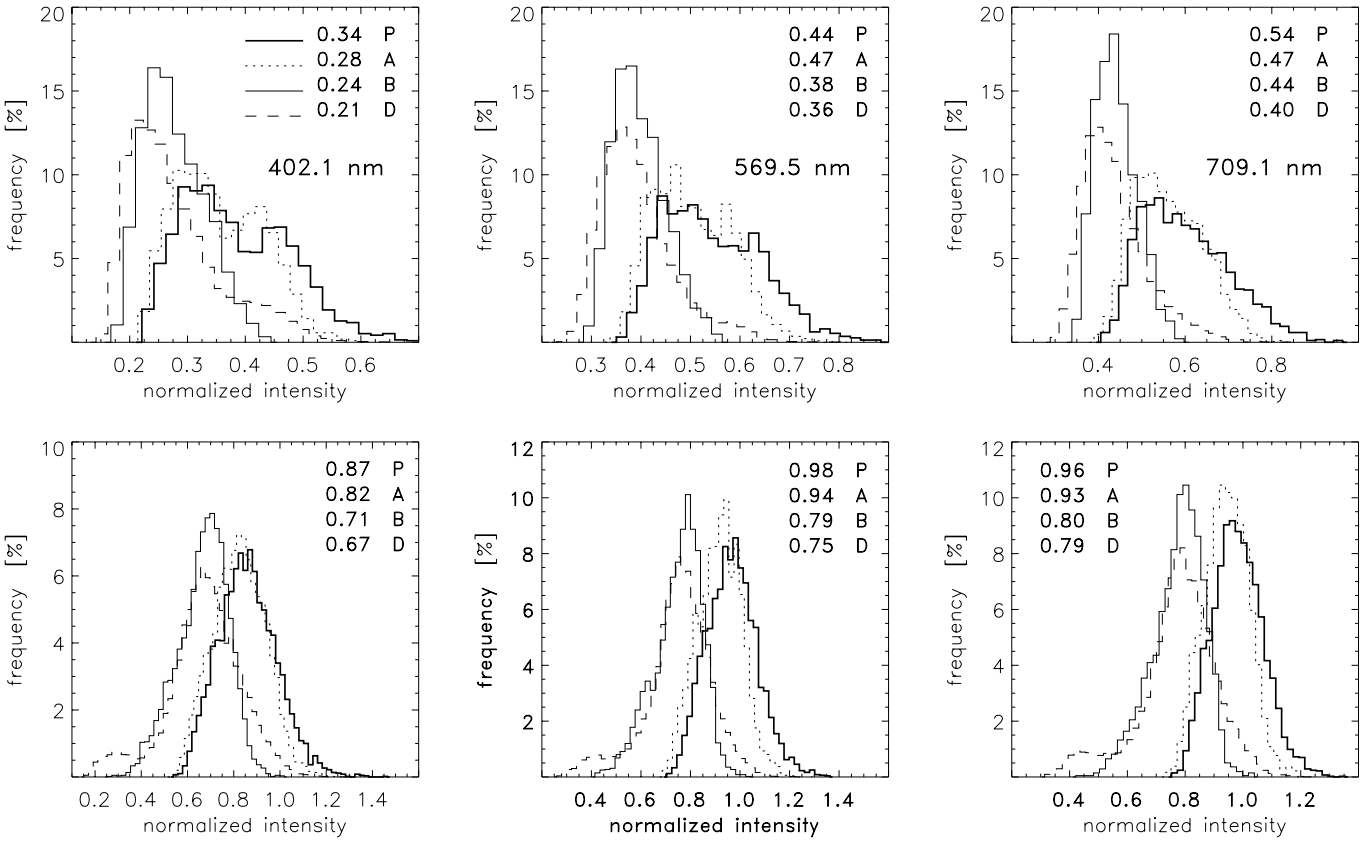

Fig. 2. Intensity distributions in the observed continuum bands inside the umbra (upper panel) and penumbra (lower panel). Bin size = 0.02. P: peak intensity (thick full line). A: average intensity (dotted line). B: average background intensity at the location of the structure (thin line). D: minimum contour intensities in the vicinity of the identified structure (dashed line). Given values refer to the maximum of the distribution function. All distributions are normalized with respect to the total number of identified structures except for the D-distribution, which is normalized with respect to the total number of minimum intensity values.

whole sequence and are normalized to the total number of structures found in the corresponding sunspot region. The distribution of the UD-intensities P and A are asymmetric and broader compared to the background intensities. Most pronounced in the blue continuum band, the shape of the P-distribution shows the contribution of two components. The two peaks are located at 0.34 (5230 K) and 0.46 (5480 K). The green continuum shows two peaks located at 0.44 (5060 K) and 0.63 (5460 K), respectively. The red continuum shows a single peak located at 0.59 (5030 K). The distribution of the individual background intensities, D, and the mean local background intensity, B, are single-peaked and asymmetric. The asymmetry is due to UDs that occur in regions with strong intensity gradients. The maximum of B is located at 0.38 (4890 K), that of D is somewhat lower at 0.36 (4910 K).

The penumbral intensity distributions of P, A, B and D (Fig. 2, lower row) are single-peaked and symmetric. Characteristic values for P and A, are located at 0.98 (5990 K) and 0.94 (5960 K), respectively. Background intensities, B and D, peak at 0.79 (5730 K) and 0.75 (5670 K), respectively. The D-distribution reveals a second component located at very low intensities. This contribution is formed by intensities that belong rather to

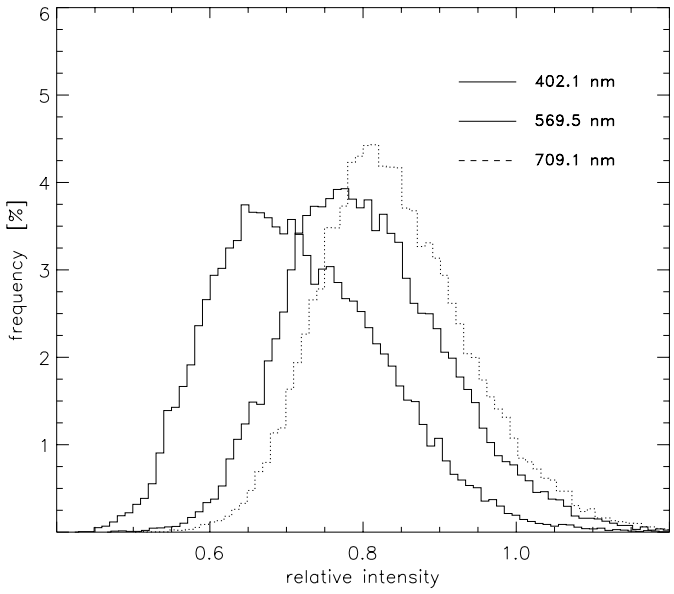

Fig. 3. Penumbral intensity distribution of one of the best images for the three observed continuum bands 402.1 nm (thick line), 569.5 nm (thin line) and 709.1 nm (dotted line). Bin size = 0.01.

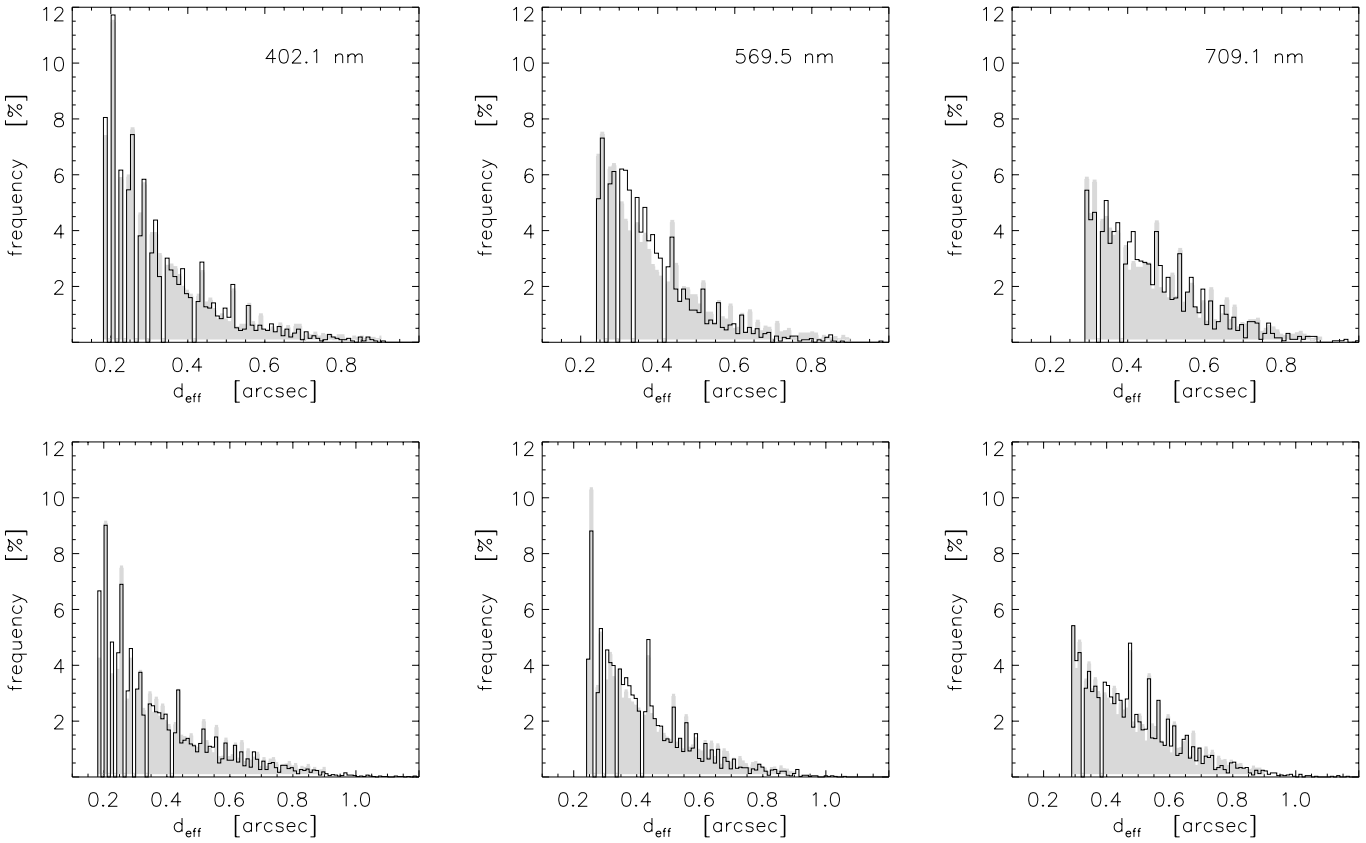

Fig. 4. Distribution of size $d_{\rm eff}$ identified structures in the three wavelength bands compared for the reconstructed (full line) and the uncorrected (shaded) data set. The distributions are normalized with respect to the total number of identified structures in the umbra and penumbra, respectively. Upper panel: umbra. Lower panel: penumbra. Bin size = 0.01 arcsec.

the umbra than to the penumbra and can be explained as follows: the FFA searches for the minimum contour line around the selected structure, which is done by following the intensity gradient until the slope changes the sign from negative to positive. Especially for PGs, this situation does not occur until umbral regions are reached. The width of the individual B- and D-distributions is about 15% and 17% of the mean quiet sun intensity, whereas the P- and A-distributions are about 20% and 17% broad.

For comparison, Fig. 3 displays the total penumbral intensity distribution for the observed continuum bands of one of the best images in our sequence. The distributions are all single-peaked and symmetric.

4.2. Size-distribution and area fractions

The size distribution of identified structures (full thick line) in the umbra and the penumbra is shown in Fig. 4. Also displayed are the distribution functions that result from the uncorrected data (indicated by the shaded area). All distribution functions reveal, independent from the wavelength and the sunspot region, the same behaviour: the distributions show no peak but an increase with decreasing size $d_{\rm eff}$ up to the diffraction limit. The shape of the distributions changes only little with the threshold intensity ΔI. The reconstructions lead to the following result: the average diameter $d_{\rm eff}$ and deviations (1σ) of UDs and PGs amounts to 0.39 ± 0.12 arcsec and 0.43 ± 0.15 arcsec, respectively. The average size changes slightly with ΔI: an increase of ΔI leads to a decrease of the average size of the structures. With regard to PGs the derived sizes must be taken as upper limits since $d_{\rm eff}$ tends to overestimate the size of an elongated structure.

Table 1. Average values and deviations of effective diameter $d_{\rm eff}$ and area fraction f for umbral and penumbral structures. Upper row: uncorrected data. Lower row: reconstructed data.

λ [nm]	**Umbra**		**Penumbra**	
	$d_{\rm eff}$	f	$d_{\rm eff}$	f
402.1	0.35 ± 0.15	0.11 ± 0.03	0.41 ± 0.19	0.15 ± 0.05
	0.35 ± 0.14	0.11 ± 0.03	0.39 ± 0.18	0.14 ± 0.05
569.5	0.41 ± 0.14	0.16 ± 0.01	0.44 ± 0.16	0.14 ± 0.02
	0.39 ± 0.12	0.13 ± 0.01	0.43 ± 0.15	0.12 ± 0.02
709.1	0.47 ± 0.14	0.16 ± 0.02	0.49 ± 0.16	0.14 ± 0.03
	0.46 ± 0.13	0.16 ± 0.02	0.48 ± 0.15	0.13 ± 0.03

From the *FWHM*-sizes, the area fraction f occupied by the structures can be calculated by the ratio of the summed area of all identified structures to the total area of the sunspot region under consideration. This quantity is very sensitive to ΔI and less sensitive to the minimum size. With a decrease of ΔI the area fraction increases,

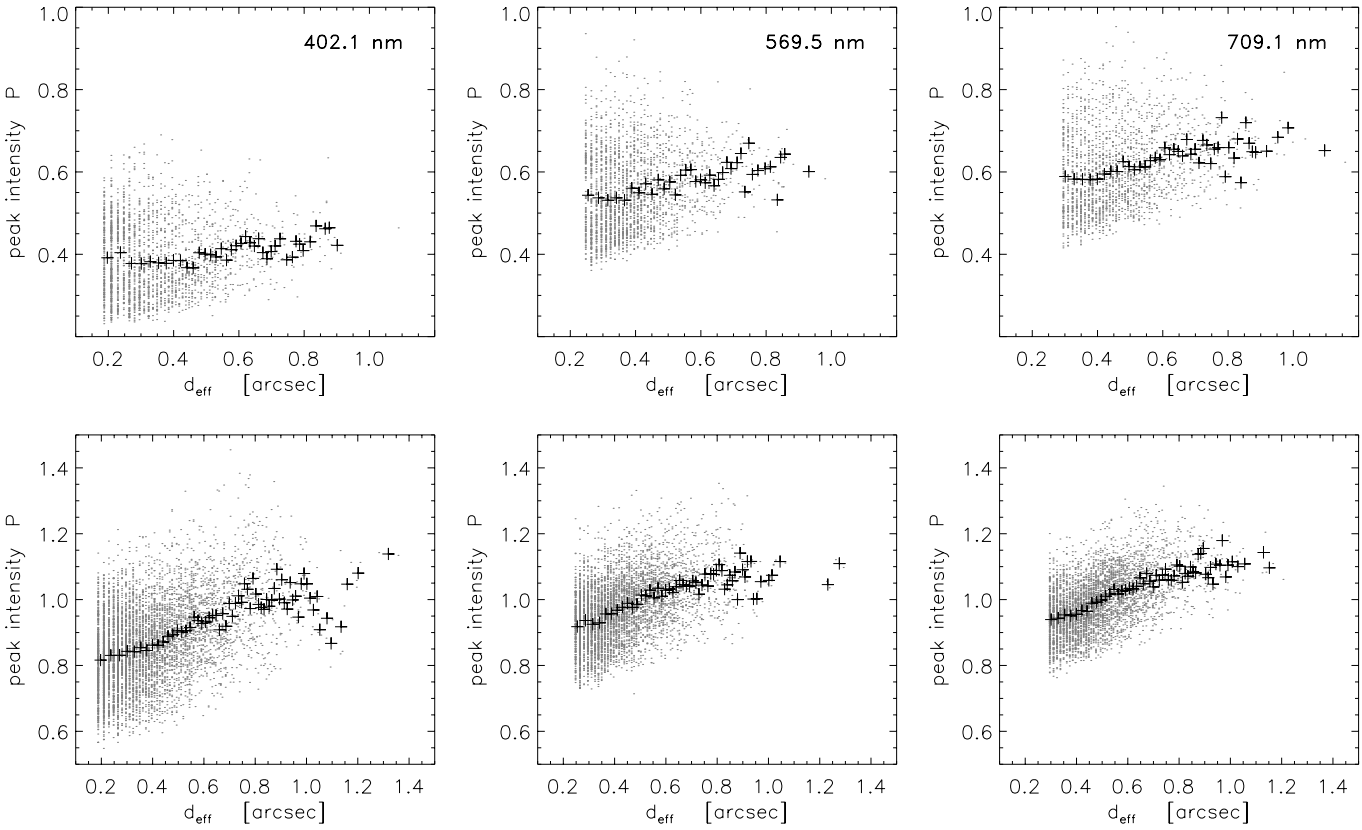

Fig. 5. Relation between peak intensity P and size $d_{\rm eff}$ in the observed wavelength bands, based on the reconstructed data set. Upper row: umbra. Lower row: penumbra.+: mean peak intensity for a binned size (UDs: bin size = 0.018 arcsec. PGs: bin size = 0.017 arcsec).

since the number of identified structures increases. Within the umbra, the area fraction triples, while within the penumbra it doubles. In particular for the penumbra these values must be regarded as lower limits. The search algorithm does not identify the whole bright filament, but only the bright head. The total area of the filament is probably three times as big. Thus, the area fraction is underestimated.

4.3. Relation between brightness and size

The relation between the peak intensity, P, and the effective diameter, $d_{\rm eff}$, is illustrated in Fig. 5 for the reconstructed data. For each identified structure of specified size, there exists a range of observed brightnesses. Thus, there exist bright as well as faint structures of equal equivalent size $d_{\rm eff}$. We follow the same procedure as described before with respect to the relation between peak intensity and mean local background intensity of identified structures (see Sect. 4.1, Fig. 1). Each size $d_{\rm eff}$ can be assigned a mean intensity, that results from an average over the corresponding range of observed brightness. These mean intensities are marked in Fig. 5 with the +-symbol. As in Fig. 1 binned +-values are displayed. In all three continuum bands, these mean intensities show a slight increase with size. For $d_{\rm eff} > 0.6$ arcsec the mean peak intensity fluctuates because large structures are less frequent than small ones. Thus, only a few points contribute to the mean peak intensity. The increase of the mean peak intensity with size is most conspicious for the penumbra. This behaviour is ascribed to the contribution of unresolved conglomerats of structures. The FFA interprets them as a large single structure. As a result, for each size there is a deficit of bright intensity structures.

4.4. Distribution of UD-intensities

As already mentioned before, the shape of the distribution of peak intensities P and averaged intensities A for UDs is very sensitive to the choice of ΔI and the minimum *FWHM*-size. The variation of the threshold intensity ($\Delta I = 0.01, 0.015, 0.02$) and the minimum size (4, 7 and 10 pixel) reveals that the two-component structure is clearly evident only for a combination of the lowest threshold intensity and a size near the diffraction limit. The peaks are located at 0.30 and 0.45, with the saddle point at 0.40. Since the size of UDs is uncoupled to their brightness, the variation of ΔI does not lead to a shift towards higher or lower intensities but to a change in UD frequency because low-contrast UDs are rejected. As a consequence the separation of the two components smears.

Figure 6 shows the distribution of UD peak intensities P as a function of wavelength and minimum size based on

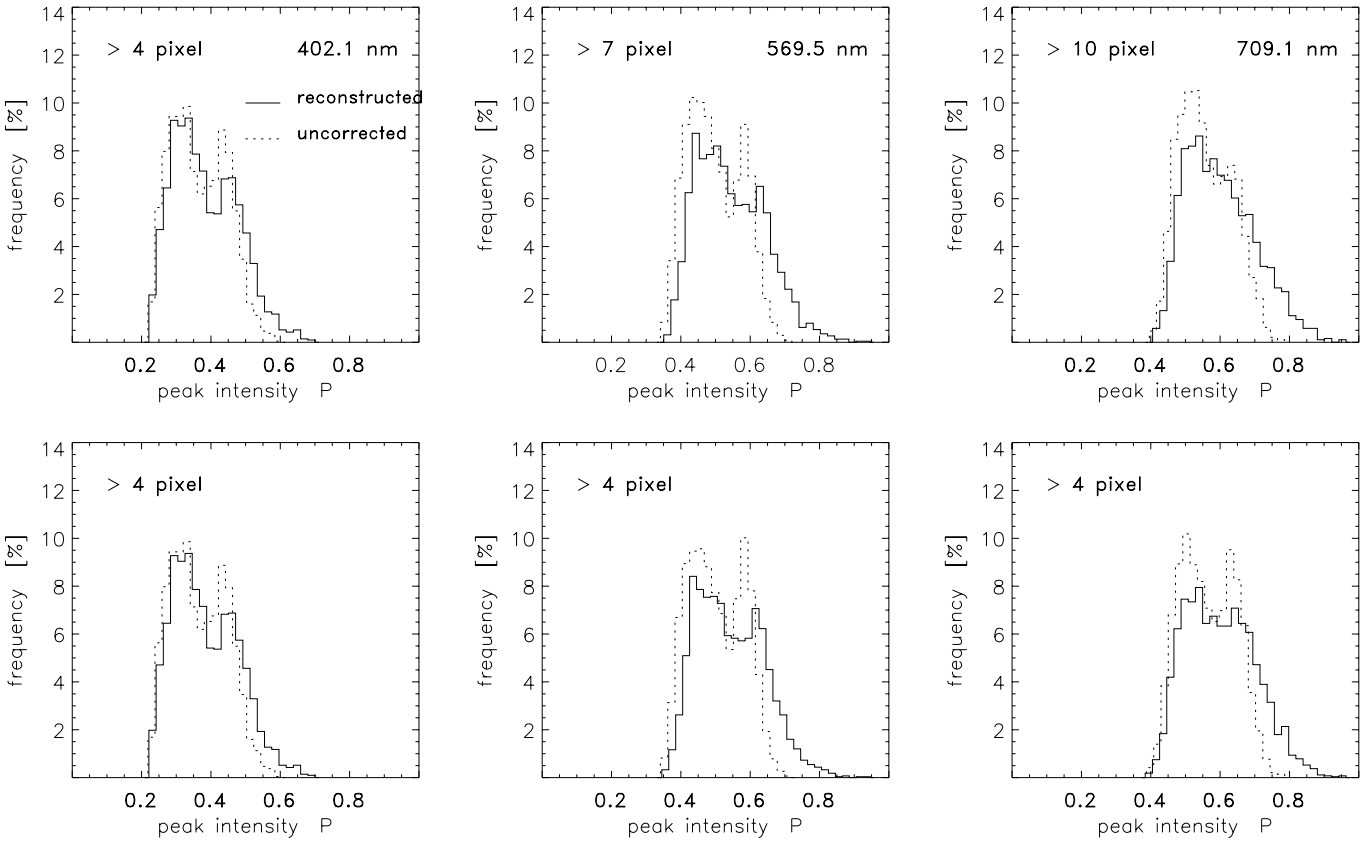

Fig. 6. Intensity distribution of UD-peak intensities for the observed continuum bands on the bases of the reconstructed (full line) and the uncorrected (dotted line) data. Upper panel: default values for the minimum size of selected UDs. Lower panel: reduced minimum size for the green and red continuum band. Bin size = 0.02.

the reconstructed and the uncorrected data set. For the default values of the minimum size, the following can be stated: the uncorrected data set leads to a double-peaked distribution of UD intensities in all three continua. In the blue and green continuum, the components (or "populations") are clearly separated. Bright and dark UDs are almost equally frequent. In the red continuum, dark UDs are more frequent than bright ones by factor of 1.5. The corresponding reconstructed intensity distributions also indicate a two-component distribution, at least for the green and blue continuum band. The image restoration dilutes the double-peak distribution, particularly in the red wavelength band. Lowering the minimum size to $\geq$4 pixel in the green and red continuum results in an increase of the number of the bright UDs. For the uncorrected data, two separated peaks with similar frequency are visible in the red continuum.

5. Discussion

5.1. Penumbral intensity distribution: bright and dark filaments

From a morphological point of view, the observed penumbra is two-component structured: bright filaments with a mean intensity $\overline{A}$ of 0.92 (5910 K) cover 14% of the total penumbral area and are separated by dark lanes of a mean intensity $\overline{D}$ of 0.76 (5670 K) (see Table 2 at the end of Sect. 6). Although the FFA was not applied to identify dark structures, we consider the average minimum-contour intensity $\overline{D}$ as a good approximation to the mean "brightness" of the dark filaments. However, we can make no statement about the size and area fraction of the dark filaments. Thus, the area fraction of the dark filaments is set to 86%, which corresponds to the area that is not occupied by bright filaments. Mean brightness and area fraction of the two components lead to a penumbral brightness of 0.78.

Krat et al. (1972) find that bright filaments typically show intensities around 0.78%, whereas dark filaments are around 0.62. Their analysis leads to the following picture: bright filaments are built up of bright chained grains, the PGs. In the inner (outer) part of the penumbra, the PGs are on average 0.90 (0.95) bright and cover approximately 43% of the penumbral area (Muller 1973). The dark filaments are on average 0.52 (0.60) bright and cover an area fraction of 57%.

The investigations of Grossmann-Doerth & Schmidt (1981) show that rather quiet penumbral regions exhibit mean intensities in the range 0.80–0.97 and 0.62–0.77 for bright and dark structures, respectively. Penumbral intensity fluctuations vary between 9.2% and 18.3%.

A photometric study of Collados et al. (1988) in the two continua at 500 nm and 550 nm yields a mean brightness of 0.85 and 0.83 for bright structures and 0.61 and 0.66 for dark structures, respectively. The corresponding area fractions amount to 49% and 51%. The average brightness of the whole penumbra therefore amounts to 0.73 and 0.74, while mean intensity fluctuations amount to 11.5% (500 nm) and 7.9% (550 nm).

Compared to former findings, in our work the area fraction occupied by the bright penumbral structures amounts to only $\sim 1/3$ of the value adopted by Muller (1973). As mentioned before (Sect. 4.2) this is due to the fact that the FFA selects primarily the bright heads of the filaments, while the extended tail of the filament is sorted out. Also, the average intensities of the dark filaments based on our analysis deviate significantly from former results. As already discussed in TS this is only partially ascribed to the influence of stray light. At first, there is growing evidence that small sunspots are brighter and hotter than large sunspots. At second, it cannot be excluded that also for small sunspots the umbral and penumbral brightness is correlated. Furthermore, the observations have been carried out during the late phase of the solar cycle, where sunspots are believed to be brighter than during the early phase of the solar cycle. This may explain the enhanced intensities of dark penumbral structures and the reduced penumbral rms-fluctuations, which amount on average to 11.3%, 9.5% and 8.8% for the blue, green and red continuum band (see TS).

In opposition to the morphological appearance, the intensity distribution of the whole penumbra at no time shows a split and a completely separated second component, apparently in contradiction to the picture of the penumbra given by Muller (1973). Our single-peaked penumbral intensity distributions, as shown in Fig. 3, rather indicate the following: what is a bright and dark filament is defined locally by the immediate penumbral vicinity. The terms bright and dark filament have only a local meaning. This is consistent with Grossmann-Doerth & Schmidt (1981) and Collados et al. (1988).

By means of a simple model of bright and dark penumbral structures, Collados et al. (1988) show that the observed single-peaked distributions are reproducable, if the mean intensity of bright and dark filaments is in the range 0.85–0.90 and 0.60–0.64, respectively, and if the individual distributions of the two components have a width $\geq$10–15% of the average quiet sun intensity. In dependence of the choice of the free parameters (width, area fraction, mean intensity) of the single components, double-peaked distributions or asymmetries appear. This result is supported by our results. Our distributions show widths that are on average $\geq$16% (bright component) and $\geq$17% (dark component). Therefore, the observed single-peaked distributions do not directly contradict the results given by Muller (1973).

5.2. Relation between brightness and background

The observed mean intensity ratios P/B for UDs are in good agreement with already existing results. Sobotka et al. (1993) find that the distribution function of the intensity ratio P/B accumulates at 1.35 with an average value and deviation of 1.56 ± 0.33. Our observations lead to an average value and deviation of 1.38 ± 0.21, with a peak of the distribution function at 1.23, which is slightly below the values of Sobotka et al. (1993). This can be ascribed to the choice of the threshold intensity ΔI. Already a $\Delta I = 0.015$ leads to higher average values of 1.42 ± 0.20 for P/B.

The sector-like shape of the relation between P and B for umbral structures is well established in all observed continuum bands and confirms former studies (Sobotka et al. 1992a, 1993). The upper edge of the sector is below a straight line of slope $\sim$3, which is assumed to be approximately the true ratio of P/B (Sobotka et al. 1992a, 1993). The established correlation bewteen P and B presents evidence that the peak intensity of UDs is related to the corresponding local umbral background. Otherwise, the UD-intensities would be distributed irregular in the halfplane above the $P/B = 1$ line.

Penumbral features are slighty less correlated to the background than umbral features. For the inner penumbra, the determination of the local background intensity is more insecure compared to the umbra, because of the steep intensity gradient. The algorithm moves too far into the umbra and therefore underestimates the average background intensity. As a result, the P/B values are overestimated. Points in the P–B diagram slide horizontally to the left side. This degrades the correlation and falsifies the relation between P and B. For the penumbra we therefore cannot exclude a dependence between P and B, similar to that of the umbra.

Figure 7 displays the distribution functions of the intensity ratio P/B for structures inside the umbra (upper panel) and the penumbra (lower panel). The distributions are single-peaked and asymmetric: they decrease rapidly to lower and slowly to higher intensities. Typical P/B values are found around the peak at 1.22 (1.17) for umbral (penumbral) features.

5.3. Brightness temperature

The identified UDs do not reach the temperature of the surroundings outside the spot. Typically, UDs are $\sim$680 K hotter than the umbral minimum and $\sim$760 K colder than the mean surroundings outside the spot. Individual UD temperatures vary between 4860–5950 K. The application of image reconstruction techniques combined with the determination of brightness temperatures provides evidence that UDs do not reach quiet sun temperatures (Bumba et al. 1990; Grossmann-Doerth et al. 1986; Sütterlin & Wiehr 1998). Pahlke & Wiehr (1990) derive a two-component model of an umbra, which reproduces spatially unresolved Stokes-V-profiles of photospheric lines

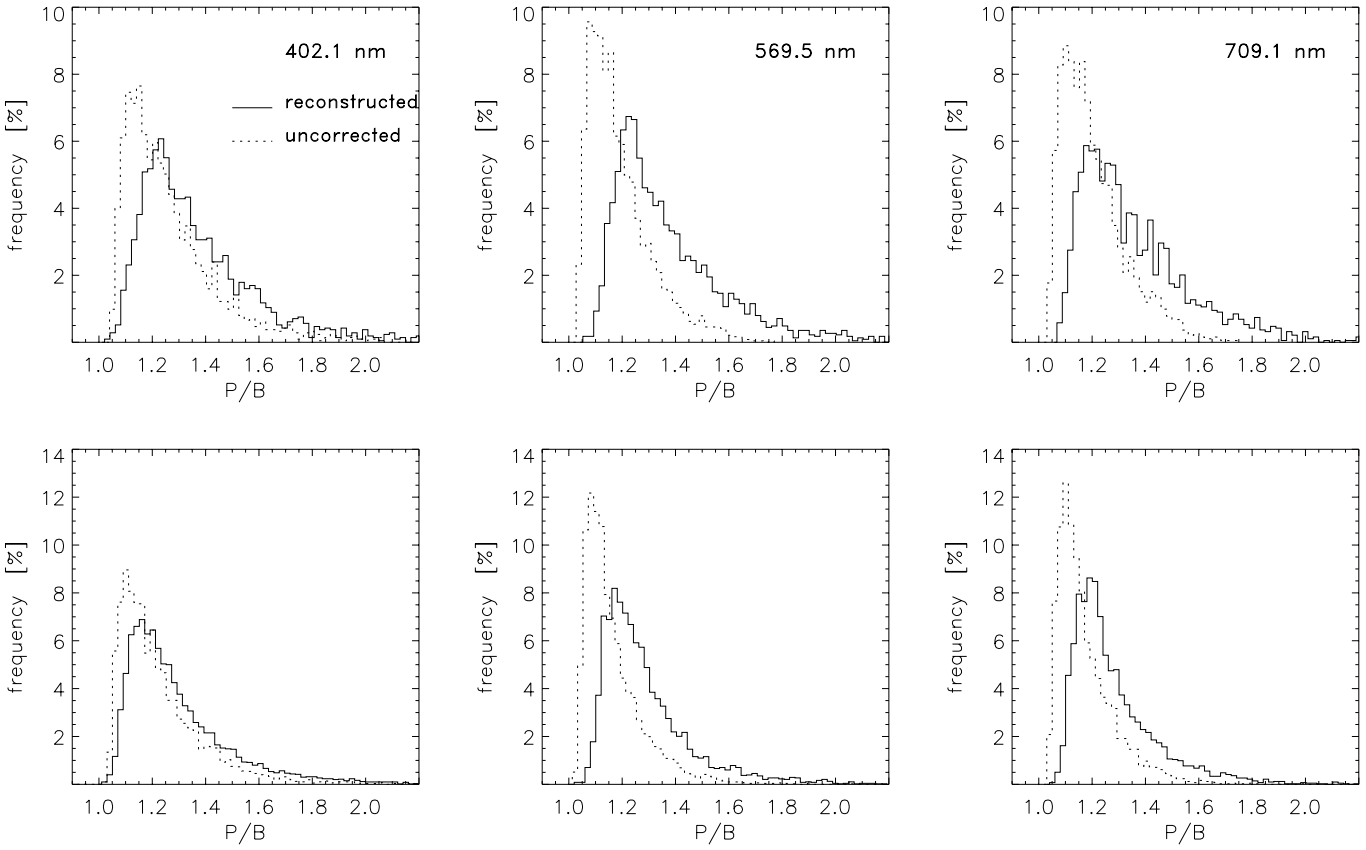

Fig. 7. Distribution of the intensity ratio P/B based on the reconstructed (full line) and the uncorrected (dotted line) data in the observed continuum bands. Upper panel: umbra. Lower panel: penumbra. All distributions are normalized with respect to the total number of identified structures. Bin size = 0.01.

and find that the UD-temperature is much less than that of the surrounding quiet sun. Thus, our results are in agreement with former findings.

In contrast hereto results from a two-color photometry and the use of color temperatures (Beckers & Schröter 1968; Koutchmy & Adjabshirzadeh 1981; Aballe-Villero 1991) show that UDs reach or exceed the temperature of the surrounding quiet sun. The difference between the use of color and brightness temperatures and the consequences have been already discussed in TS. Here we just want to remind the reader that observed color temperatures above quiet sun values do not imply that UDs have brightness temperatures higher than the photosphere outside the sunspot.

Some of the PGs show exceptionally high brightness temperatures: they exhibit temperatures in the range 5990 ± 140 K, close to the photospheric conditions of the surroundings outside the spot. Maximum temperatures are reached at 6490 K, which is 450 K above the mean quiet sun temperature and as hot as the brightest granule (6500 K) in our field of view. This confirms recent results (Sütterlin & Wiehr 1998) and predictions of numerical simulations (Schlichenmaier et al. 1998). In accordance with magneto-hydrodynamical simulations, the penumbral structure is dominated by the dynamcis of ascending flux tubes. In this picture, the PGs are interpreted as the intersection of these flux tubes with the ($\tau = 1$)-level. The flux tubes, heated by a systematic flow (Evershed flow), establish temperatures even higher than the hottest granules. The optically thick bright filaments correspond to the radiative signature of the horizontally outflowing hot plasma channeled by the flux tube. During the outflow the plasma cools until the filament becomes optical thin and cannot be distinguished from the dark background. This leads to the characteristic tail of the bright filaments. Since the hot flux tube is embedded in a cool surrounding it cools by radiative heat exchange (Schlichenmaier et al. 1999) and leads to a slight heating of the background. To which extent this heating or cooling of the flux tubes can account for the observed brightness of the dark filaments – and the single-peaked penumbral intensity distributions – needs further investigation. In principle, it is conceivable that the brightness of the penumbral background is a consequence of this heating mechanism due to the cooling of the flux tubes. However, the cooling must account for a mean flux difference between the umbral and penumbral background of approximately 40%.

5.4. Filling with UDs

The area fraction occupied by UDs can be determined directly on the basis of the observed size and number of

UDs per umbra, but the dependence from data quality and the identification criteria is obvious. The observed area fractions lie in the range of 6–18%. Rather dark umbrae show a somewhat lower percentage (6–8%) than brighter umbrae (10–15%) (Sobotka et al. 1993). Sobotka et al. (1997a) obtain a similar result ($8.9 \pm 1.5\%$). Therefore, our results based on the reconstructed ($\sim$13.1%) and the uncorrected data ($\sim$15.8%) fit well into already existing results, if we keep in mind that the observed sunspot is rather small and bright (see TS). An untypical high area fraction of 30% for a small umbra, found by Sobotka et al. (1988), was due to the moderate resolution of the data set. Spectroscopic investigations lead to somehow lower area fractions of $\sim$5% (Adjabshirzadeh & Koutchmy 1983; Pahlke & Wiehr 1990).

5.5. Size distributions

The determination of UD sizes is still a challenge, which is reflected in the huge amount of different methods to measure the UD size or to infer the true size of UDs. Among these are image reconstruction techniques and stray light corrections (Adjabshirzadeh & Koutchmy 1978, 1980; Grossmann-Doerth et al. 1986), the application of identification algorithms, the two-color photometry (Beckers & Schröter 1968; Koutchmy & Adjabshirzadeh 1981; Aballe-Villero 1991) or a combination of the individual methods (Sobotka et al. 1993, 1997a). Accordingly, the results vary on a wide range (0.3–0.6 arcsec Aballe-Villero 1991, 0.3–1.4 arcsec Grossmann-Doerth et al. 1986). The present work confirms and supplements the work of Sobotka et al. (1997a).

Our observed sizes on the basis of an effective diameter vary over a wide range, depending on the selection criteria. The choice of a threshold intensity just above the noise level results in effective diameters of 0.25–0.98 arcsec. Most probably, the largest UD proxies correspond to conglomerates of UDs that cannot be separated by the FFA. However, the existence of very large UDs cannot be excluded. Grossmann-Doerth et al. (1986) report about specimen with diameters up to 1.4 arcsec. The distribution of the UD size, $d_{\rm eff}$, features an increase towards the diffraction limit: the smaller the structures, the more numerous they are. This means, that the UDs cannot be assigned to a typical size, since the spatial resolution is not sufficient to resolve the smallest UDs. From the steep increase towards the diffraction limit can be inferred, that the size of an UD is not far below the diffraction limit (Sobotka et al. 1997a). The authors find an average UD-size of 0.42 ± 0.12 arcsec.

Our analysis leads to UD-sizes that are in agreement with the aforementioned results: UDs show average diameters of 0.39 ± 0.12 arcsec for the reconstructed data and 0.41 ± 0.14 arcsec for the uncorrected data. In a similar investigation Sobotka et al. (1993) find a mean UD-diameter of 0.43 ± 0.10 arcsec. Their corresponding size distribution of the observed UDs is symmetric and single-peaked with a maximum at 0.4 arcsec which is above the spatial resolution in the data (0.3 arcsec, 240 km). Adjabshirzadeh & Koutchmy (1983) obtain a one-component size distribution with a maximum at 0.225 arcsec (165 km) for a single spot with only the brightest UDs considered. The shape of the size distribtuion function obviously depends on the volume of the UD-sample, the noise level, the spatial resolution of the data set and of the UD-identification method (by visual inspection or automatic).

The comet-like shaped heads of the bright filaments, the PGs (Muller 1973), are on average 0.35 arcsec wide and 0.5–2.0 arcsec long (Krat et al. 1972; Muller 1973; Moore 1981; Bonet et al. 1982). Based on a statistical analysis of the penumbral fine structure Grossmann-Doerth et al. (1986) give 0.55 arcsec as an upper limit for the size of the bright and dark filaments. Altogether, penumbral spatial scales are close to the diffraction limit. Our analysis leads to somewhat bigger penumbral scales: on average the bright filaments show effective diameters of 0.43 ± 0.15 arcsec (reconstructed) and 0.44 ± 0.16 arcsec (uncorrected). As stated before, the effective diameter overestimates the size of an elongated structure. The size distribution of the PGs shows the same behaviour as that for the UDs: an increase towards the diffraction limit, which suggests that the smallest penumbral structures are still unresolved.

5.6. UD-populations

The distribution function of UD peak intensities P and the average UD intensities A is double-peaked with two well-separated maxima in all observed continua for the uncorrected data set. The appearance of the double peak is very sensitive to the choice of the threshold intensity ΔI and the minimum size. Only for values of ΔI and the minimum size near the noise level and the diffraction limit respectively, the two UD-populations are distinguishable. The intensities accumulate approximately at 0.32 and 0.45. In the reconstructed data set for the red continuum, the double-peaked distribution does not appear until the minimum size is set below the diffraction limit for the red wavelength. If the positions are checked, it can be shown that the members of the hot population are settled at the edge of the umbra and on a streak combining the lightbridge with the penumbra on the opposite side. Members of the cool population are located in the central regions of the umbra. However, the overall distribution of UDs inside the umbra is irregular, but not random. There are regions which are void of UDs. In these regions, UDs neither pop up nor existing UDs manoeuvre into. An example is the darkest part of the umbra. Figure 8 illustrates this behaviour for the reconstructed data set. The UDs with a peak intensity of $P > 0.4$ are marked with +-symbols and those with $P < 0.4$ are marked with $\diamond$-symbols. Unlike the distribution functions of P and A, the distribution functions of the intensity ratios P/B and $(P - B)/B$ reveal no second component. These ratios do

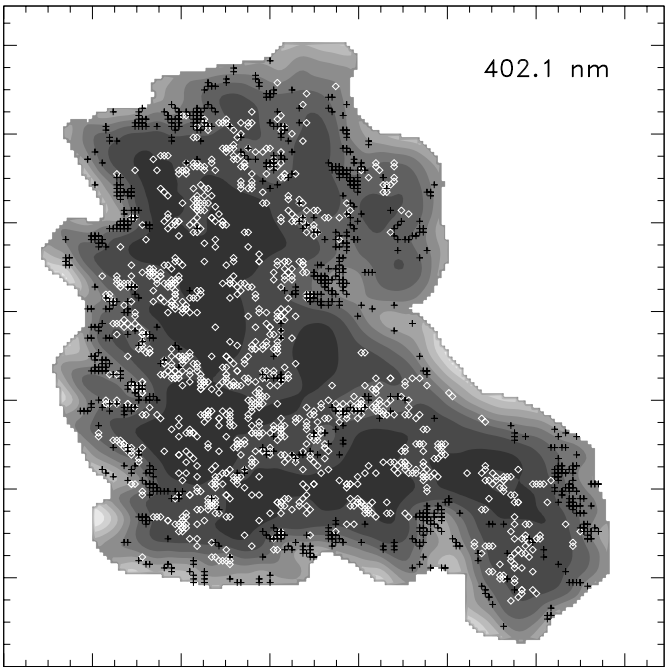

Fig. 8. UD-population inside the umbra (image scale: 1 minor tickmark $\widehat{=}$ 0.5 arcsec). +: bright component. ⋄: dark component.

no longer contain the information about the position of the UD inside the umbra.

A similar study was carried out by Sobotka et al. (1997b). The authors consider the distribution function of time-averaged UD peak intensities. This distribution function shows two separated maxima located at 0.34 and 0.48, which differs only slightly from our results for the blue continuum.

The relation between the UD peak intensity and the local background suggests the following: the brightest UDs are located where the background is high or marked by an intensity gradient (lightbridge, near penumbra). The brightness or temperature of UDs appears to be controlled or at least influenced by the background intensity or another physical quantity which characterizes the background. Thus, in central located UDs energy is transported less efficient compared to peripheral located UDs. The existence of two different populations was a priori assumed by Grossmann-Doerth et al. (1986), who differentiated between peripheral UDs (PUDs) and central UDs (CUDs) according to their location inside the umbra. The close proximity to the penumbra raises the question whether the pre-defined PUDs and the members of the bright population – at least those which are located at the boundary to the penumbra – are remnants of former penumbral filaments. In order to verify this, sufficient long time sequences of high spatial resolution covering all evolutionary states of sunspot penumbral filaments are needed.

6. Conclusions

We summarize our findings as follows:

1. The spatial distribution of UDs is not random. There exist regions inside the umbra, that are preferred or avoided by UDs. The distribution function of UD temperature is double-peaked, giving evidence for two UD populations with different efficiency of energy transport. Members of the hot population are mainly located where the temperature of the local background is enhanced or features a gradient. This is in particular the case for the near-edge regions of the umbra. Members of the cold population are mainly concentrated in the central regions of the umbral nuclei.
2. The observed UDs do not reach the temperature of the surrounding photosphere outside the spot.
3. The presently available spatial resolution is not sufficient to characterize the observed small-scale structures by their size. The frequency of structures increases strongly towards spatial scales near the diffraction limit. The smallest structures inside the umbra and penumbra are still unresolved, but are believed to concentrate just below the diffraction limit.
4. The energy transport in PGs appears to be very efficient: typically, the heads of the optical thick part of the filaments are brighter than the mean surrounding photosphere outside the sunspot. Individual PGs reach or even exceed the temperature of the brightest granules in the immediate surrounding of the sunspot.
5. Based on the intensity distribution inside the penumbra, the existence of a second component cannot be completely excluded. However, there is evidence, that the terms “bright filament” and “dark filament” have only a local meaning.
6. The observation of higher-than-average temperatures of PGs and the as single-peaked classified intensity distribution inside the penumbra together with the results of numerical simulations suggest the following magneto-hydrodynamical scenario: the filamentary structure of the penumbra originates from the dynamics of ascending flux tubes. Due to a systematic flow (Evershed-flow) these flux tubes are heated and protrude against the surrounding (background). The highest temperature is reached at the point where the flux tube crosses the ($\tau = 1$)-line. This cross section defines the PG. The radiative signature of the horizontally outflowing hot plasma channeled by the flux tube, is interpreted as a bright optical thick filament. In this picture the dark filaments are identified with the space that is not filled with the hot flux tubes, meaning the optical thin part of the flux tube. The temperature of the dark background is influenced by the cooling of hot flux tubes in the vicinity.

Despite the numerous observational results for umbral and penumbral fine structure, the need for further investigations is obvious. Some of the key questions are: (a) what leads to the different UD-populations? (b) What is the

Table 2. Umbral and penumbral intensities (upper row) and the corresponding brightness temperatures (lower row, given in K) in the observed continuum bands. The index $-(+)$ refers to the minimum (maximum) of the measured values. Deviations correspond to one standard deviation (1σ). The $\widehat{X}$ denotes the maximum of the distribution of the quantity X.

	Umbra				Penumbra			
λ [nm]	$(P)_-$	$(P)_+$	$\overline{P}$	$\widehat{P}$	$(P)_-$	$(P)_+$	$\overline{P}$	$\widehat{P}$
402.1	0.23	0.69	0.39 ± 0.09	0.34	0.55	1.45	0.87 ± 0.12	0.84
	4980	5880	5350 ± 180	5270	5670	6690	6090 ± 150	6100
569.5	0.36	0.94	0.55 ± 0.09	0.44	0.71	1.35	0.97 ± 0.10	0.98
	4860	5950	5280 ± 190	5220	5590	6490	5990 ± 140	6000
709.1	0.42	0.95	0.60 ± 0.09	0.54	0.76	1.34	0.99 ± 0.09	0.96
	4730	5830	5170 ± 200	5040	5490	6450	5900 ± 140	5860
λ [nm]	$(A)_-$	$(A)_+$	$\overline{A}$	$\widehat{A}$	$(A)_-$	$(A)_+$	$\overline{A}$	$\widehat{A}$
402.1	0.22	0.59	0.36 ± 0.07	0.28	0.53	1.23	0.83 ± 0.11	0.83
	4950	5720	5300 ± 160	5460	5640	6450	6040 ± 130	6070
569.5	0.35	0.80	0.51 ± 0.08	0.47	0.70	1.21	0.92 ± 0.08	0.94
	4830	5670	5200 ± 150	5110	5500	6310	5910 ± 130	5930
709.1	0.40	0.82	0.56 ± 0.07	0.53	0.74	1.18	0.94 ± 0.07	0.93
	4690	5550	5080 ± 160	4990	5450	6190	5820 ± 120	5800
λ [nm]	$(B)_-$	$(B)_+$	$\overline{B}$	$\widehat{B}$	$(B)_-$	$(B)_+$	$\overline{B}$	$\widehat{B}$
402.1	0.18	0.43	0.28 ± 0.05	0.24	0.26	1.01	0.67 ± 0.11	0.72
	4800	5450	5100 ± 120	5030	5040	6260	5830 ± 170	5910
569.5	0.29	0.55	0.40 ± 0.05	0.38	0.42	1.03	0.76 ± 0.10	0.80
	4640	5290	4950 ± 110	4900	5000	6080	5660 ± 170	5700
709.1	0.35	0.59	0.44 ± 0.04	0.44	0.43	1.03	0.77 ± 0.09	0.79
	4550	5140	4800 ± 110	4790	4760	5950	5510 ± 170	5570
λ [nm]	$(D)_-$	$(D)_+$	$\overline{D}$	$\widehat{D}$	$(D)_-$	$(D)_+$	$\overline{D}$	$\widehat{D}$
402.1	0.15	0.64	0.28 ± 0.08	0.21	0.16	1.27	0.68 ± 0.16	0.66
	4710	5830	5110 ± 190	4950	4820	6390	5840 ± 240	5830
569.5	0.24	0.80	0.40 ± 0.07	0.36	0.27	1.27	0.76 ± 0.13	0.76
	4510	5760	4960 ± 170	4930	4670	6220	5670 ± 230	5670
709.1	0.30	0.85	0.44 ± 0.07	0.40	0.32	1.24	0.78 ± 0.13	0.80
	4390	5670	4800 ± 180	4720	4570	6140	5540 ± 240	5500
λ [nm]	$(P/B)_-$	$(P/B)_+$	$\overline{P/B}$	$\widehat{P/B}$	$(P/B)_-$	$(P/B)_+$	$\overline{P/B}$	$\widehat{P/B}$
402.1	1.03	2.82	1.39 ± 0.25	1.23	1.02	2.94	1.31 ± 0.22	1.16
	1.00	1.17	1.05 ± 0.03	1.02	1.00	1.19	1.05 ± 0.03	1.02
569.5	1.06	2.46	1.38 ± 0.21	1.22	1.03	2.77	1.30 ± 0.17	1.17
	1.01	1.21	1.07 ± 0.03	1.04	1.01	1.26	1.06 ± 0.03	1.04
709.1	1.08	2.48	1.36 ± 0.20	1.18	1.05	2.73	1.29 ± 0.16	1.19
	1.02	1.25	1.08 ± 0.04	1.04	1.02	1.30	1.07 ± 0.03	1.05

regulating mechanism responsible for the appearence and disappearance of UDs? (c) What is the real size of UDs and PGs? (d) What is the fundamental relation between the intensity of UDs and the local background? Over and above the morphological studies presented herein, spectroscopic and polarimetric measurements are needed to determine the magnetic field configuration and the flows at the scale of umbral and penumbral structures. With the availibity of adaptive optics and suitable postfocus instruments, these questions could be answered in a near future.

Acknowledgements. The authors wish to thank Rolf Schlichenmaier for his inspiring help in trying to understand what the penumbra is telling us from a theoretical point of view. We are deeply grateful to Mats Löfdahl for his support during the "fights" with phase diversity. Thanks to Scott Acton for his introduction into observational and computational aspects of the image reconstruction technique. We feel indebted to Thomas Kentischer, observations would not be possible without his manpower. We thank Michael Knölker for his contributions and for financial support (for AT) granted by the High Altitude Observatory. Part of this work was supported by the German *Deutsche Forschungsgemeinschaft, DFG.*

References

Aballe Villero, A. M. 1991, in Sunspots: Theory and Observations, ed. J. H. Thomas, & N. O. Weiss (Kluwer)

Adjabshirzadeh, A., & Koutchmy, S. 1978, Compt. Rendus, 286, 23, 335

Adjabshirzadeh, A., & Koutchmy, S. 1980, A&A, 89, 88

Adjabshirzadeh, A., & Koutchmy, S. 1983, A&A, 122, 1

Beckers, J. M., & Schröter, E.-H. 1968, Sol. Phys., 4, 303

Bonet, J. A., Ponz, J. D., & Vázquez, M. 1982, Sol. Phys., 77, 69

Bumba, V., Sobotka, M., & Simberová, S. 1990, in The dynamic sun, Publ. Debrecen Heliophys. Obs. 7, ed. L. Deszø, 84

Choudhuri, A. 1986, ApJ, 302, 809

Collados, M., del Toro, J. C., & Vázquez, M. 1988, A&A, 195, 315

Denker, C., de Boer, C. R., Volkmer, R., & Kneer, F. 1995, A&A, 296, 567

Denker, C. 1998, Sol. Phys., 180, 81

Grossmann-Doerth, U., & Schmidt, W. 1981, A&A, 95, 366

Grossmann-Doerth, U., Schmidt, W., & Schröter, E.-H. 1986, A&A, 156, 347

Harvey, J. W., & Breckinridge, J. B. 1973, ApJ, 182, L137

Kentischer, T. 1995, A&AS, 109, 553

Knobloch, E., & Weiss, N. O. 1984, MNRAS, 207, 203

Koutchmy, S., & Adjabshirzadeh, A. 1981, A&A, 99, 111

Krat, V. A., Karpinsky, V. N., & Pravdjuk, L. M. 1972, Sol. Phys., 26, 305

Lites, B. W., Bida, T. A., Johannesson, A., & Scharmer, G. B. 1991, ApJ, 373, 683

Lites, B. W., Skumanich, A., & Scharmer, G. B. 1990, ApJ, 355, 329

Moore, R. L. 1981, ApJ, 249, 390

Moreno-Insertis, F., & Spruit, H. C. 1989, ApJ, 342, 1158

Muller, R. 1973, Sol. Phys., 32, 409

Obridko, V. N. 1975, Sov. Astronomy, 18, 758

Parker, E. N. 1979a, ApJ, 230, 905

Parker, E. N. 1979b, ApJ, 234, 333

Pahlke, K.-D., & Wiehr, E. 1990, A&A, 228, 246

Sánchez Almeida, J. 1998, ApJ, 497, 967

Sánchez Almeida, J., & Bonet, J. A. 1998, ApJ, 505, 1010

Schlichenmaier, R., Jahn, K., & Schmidt, H. U. 1998, A&A, 337, 897

Schlichenmaier, R., Bruls, J. H. M. J., & Schüssler, M. 1999, A&A, 349, 961

Simon, G. W., Brandt, P. N., November, L. J., Scharmer, G. B., & Shine, R. A. 1994, in Solar surface magnetism, ed. R. J. Rutten, & C. J. Shrijver (Kluwer)

Sobotka, M., Bonet, J. A., & Vázquez, M. 1993, ApJ, 415, 832

Sobotka, M., Bonet, J. A., & Vázquez, M. 1992a, A&A, 257, 757

Sobotka, M., Bonet, J. A., & Vázquez, M. 1992b, A&A, 260, 437

Sobotka, M., Brandt, P. N., & Simon, G. W. 1997a, A&A, 328, 682

Sobotka, M., Brandt, P. N., & Simon, G. W. 1997b, A&A, 328, 689

Stachnik, R. V., Nisenson, P., & Noyes, R. W. 1983, ApJ, 271, L37

Sütterlin, P., & Wiehr, E. 1998, A&A, 336, 367

Tritschler, A., & Schmidt, W. 2002, A&A, 383, 1093

Weiss, N. O. 1990, MNRAS, 245, 434